Mixed Stepping / Scanning Mode Control of Stick-Slip SEM-integrated Nano-robotic Systems

Raouia Oubellil, Alina Voda, Mokrane Boudaoud, Stéphane Régnier

Mixed Stepping / Scanning Mode Control of Stick-Slip SEM-integrated Nano-robotic Systems

R. Oubellil[1,*], A. Voda[1], M. Boudaoud[2] and S. Régnier[2]

[1]*GIPSA-lab, Control Systems department, ENSE3 bat B, BP 46, Domaine Universitaire, 38400 Saint Martin d'Heres, France*

[2]*Sorbonne Université, Institut des Systèmes Intelligents et de Robotique, UMR 7222, ISIR, F-75005 Paris, France*

Abstract

The ability to do dexterous automated and semi-automated tasks at the micro- and nano-meter scales inside a Scanning Electron Microscope (SEM) is a critical issue for nanotechnologies. SEM-integrated nano-robotic systems with several Degrees Of Freedom (DOF) and one or several end-effectors have therefore widely emerged in research laboratories and industry. The Piezoelectric Stick-Slip (PSS) is one of the best actuation principle for SEM-integrated nano-robotic systems as it has two operating modes, namely a coarse positioning mode with long travel range, and a fine positioning mode with a resolution of the order of the nanometer. The main contribution of this paper is the design of a switch control strategy to deal efficiently and in a transparent way from the user's point of view, with the transition between the coarse and the fine operating modes of PSS actuators. The aim is to be able to perform positioning tasks with a millimeter displacement range and a nanometer resolution without worrying about the mode of operation of the actuator. The coarse mode and the fine mode are respectively controlled with a frequency/voltage proportional control and a H_∞ control. The switch control is based on an internal model of the actuator. Experimental results show the effectiveness of the new mixed coarse/fine mode control strategy to satisfy closed-loop stability and bumpless specifications at the switching time. For the best knowledge of the authors, this result is the first demonstration of such a control capability for PSS actuators.

1. Introduction

SEM-integrated nano-robotic systems have widely emerged in recent years to address the issue of automated and semi-automated tasks for nanotechnologies. The SEM is particularly interesting because it provides a visual feedback with nanometer resolution and a depth of field better than that of light microscopes. Nano-robotics inside the SEM enables *in-situ* tasks at the nanometer scale such as nano-manipulation [1, 2], nano-assembly [3, 4] as well as electrical [5] and mechanical characterization [6] of materials and biological samples at the small scales. SEM integrated nano-robotic systems have to be able to generate two motion modes, namely a coarse positioning with a displacement range of several micrometers or millimeters to bring an end effector close to the micro/nano-object to be manipulated, and a fine positioning with a resolution in the nanometer range to locally characterize and/or manipulate the object. According to the literature, such robots are generally actuated by piezoelectric inertial actuators in the coarse and the fine modes independently [3, 7, 5, 4, 1]. Particularly, the basic architecture of Piezoelectric Stick-Slip (PSS) type actuator [3, 7, 5] is composed of a Piezoelectric Element (PE), a slider, and a friction material between the PE and the slider. It operates in scanning mode when there is no slip between the PE and the slider, and in stepping mode when several sequences of stick and slip phases occur. In scanning mode, the PSS actuator can perform a fine positioning with a nanometer resolution but the displacement range is limited by the maximal deformation of the PE (~ few micrometers). In stepping mode, a coarse positioning with a millimeter displacement range can be achieved, but with a poor resolution. In this mode, the input voltage is usually a sawtooth signal.

The state of art has shown that PSS actuators have a real potential for nano-robotics. Design issues have been deeply investigated [8]. However, several control issues related to the nonlinear behavior and the hybrid operating mode of these actuators still require studies in order to satisfy the demanding performance in nanotechnologies. Existing control strategies can be classified into control in scanning mode and control in stepping mode. The objective of the control in scanning mode is to reduce the hysteresis effect and to damp the vibrations [9]. Hysteresis may induce open-loop positioning errors as high as 10%-15% of the displacement range [10]. Furthermore, significant oscillations of a hundred nanometers at the fundamental resonance frequency can be observed in the slider displacement [11]. These mechanical vibrations present a major problem in nano-robotics. For instance, for *in situ* stiffness measurements on membranes of 200 nm thickness [12], an oscillation of 100 nm of the end-effector can produce the membrane destruction. Open-loop strategies can be used for hysteresis compensation [13, 14] [15, 16, 17] and vibration damping [18, 19]. However,

☆This work was not supported by any organization.

*Corresponding author

Email address: raouia.oubellil@gmail.com (R. Oubellil)

in practice, it is difficult to obtain precise compensators, and hence to guarantee positioning accuracy. Also, these methods are not robust against hysteresis variations and shifts in the resonance frequency. For these reasons, numerous closed-loop control strategies have been studied in the literature, including pole-placement [20], PID control [21], H_∞ control [22, 23] [24], sliding mode control [25], LQG control [26], and so on. On the other hand, few techniques exist in the literature to control PSS actuators in stepping modes. A frequency proportional controller is proposed in [27] where the frequency of the sawtooth control voltage is chosen based on the tracking error. A cascade controller is designed via dehybridization in [28] using a hybrid model of the actuator. In the inner-loop, a hybrid controller is designed to impose a time-scale separation between continuous and discrete states. In the outer-loop, a continuous proportional derivative controller is developed using an approximated continuous model of the inner-loop in order to satisfy closed-loop stability. A frequency/amplitude proportional controller is presented in [29] to control the amplitude and the frequency of the sawtooth control signal separately. The proportional gains are determined in the same way as for classical proportional controllers. None of the existing controllers has dealt with the stepping/scanning switch problem of PSS actuators. In fact, this switch generally leads to closed-loop instability and significant vibrations at switching time, which compromises the use of these actuators for fully-automated tasks inside a SEM.

This paper focuses on a new control strategy able to drive a PSS actuator in closed loop in both stepping and scanning modes while guaranteeing an efficient bumpless switch between these two operating modes. The experimental setup used to validate the proposed strategy is a nano-robotic platform made up of a Cartesian structure actuated by PSS actuators (Fig. 1). In our approach, these actuators are initially controlled separately in scanning mode and in stepping mode. The hybrid controller involves a H_∞ scanning mode controller, a frequency/ amplitude (f/u) proportional stepping mode controller, and a switching strategy using an internal model of the actuator. Experimental results demonstrate the effectiveness of the new hybrid controller and its ability to achieve millimeter range motion with a resolution of the order of the nanometer. The closed-loop system enables automated coarse/fine positioning which opens new perspectives on the use of PSS actuators in nano-robotics, particularly to perform precise automated tasks inside a SEM.

The paper is structured as follows. In Section 2, the experimental setup used in this study is described. Sections 3 and 4 deal respectively with the scanning control and the stepping control strategies. In section 5, the new mixed stepping/scanning mode controller is presented. Section 6 concludes the paper.

2. Experimental setup

The experimental setup of the laboratory enables SEM manipulation and characterization tasks [12]. It consists of a SEM, a multi-Degrees Of Freedom (DOF) nano-robotic system including the 3 axes serial nanorobot that is studied in this paper

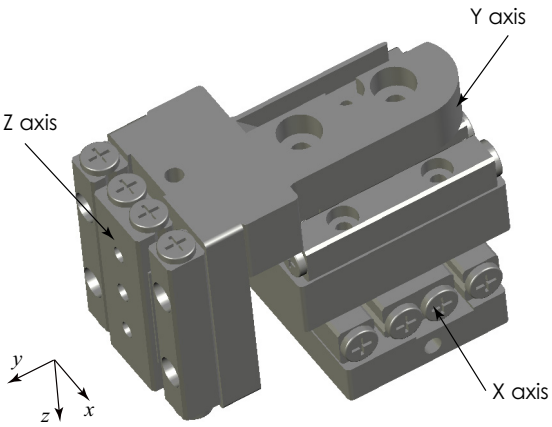

Figure 1: The 3-DOF Cartesian nano-robotic structure. It is composed of three axes X, Y and Z. Each axis is actuated by a piezoelectric stick slip actuator (SmarAct SLC-1720-S-HV).

(Fig. 1), a processor board and a human-robot interface. The processor board features a QorlQ P5020 dual-core processor running at 2 GHz. The serial nano-robotic system is actuated by PSS actuators of the same reference (SLC-1720-S-HV). Each actuator integrates an optical encoder sensor with a resolution of 20 μm. Digital interpolators with an interpolation factor of 4096 are used to obtain a measurement resolution of 5 nm.

The allowable input voltage for each PSS actuator is 0-100 V. In scanning mode, the maximum displacement of the actuators is around 2 μm, whereas it is around 12 mm in stepping mode. The hypotheses of the study are that the PE is attached to the base of the actuator, there is a friction material without lubricant between the PE and the slider and each axis (*i.e.* slider + the supported robot axis) is guided by a linear guideway, which allows only a translational motion [11].

3. Robust control in scanning mode

The scanning mode controller has to deal with hysteresis and undamped resonant modes. The standard H_∞ control strategy is designed for X, Y, and Z axes of the Cartesian structure based on the models presented in the work [30].

The desired closed-loop multi-criteria performance is threefold: (i) A closed-loop response time of few milliseconds only to deal with the need to perform fast positioning tasks in nano-robotics. To do so, the closed-loop bandwidth must be very close to the fundamental open-loop resonance frequency. (ii) A high resolution positioning with a static error of few nanometers only. This performance is fundamental in several micro/nano-robotic tasks such as nano-assembly and nanomaterial characterization. (iii) A closed-loop stability robustness against the hysteresis and the uncertain measurement time delay varying in a defined interval.

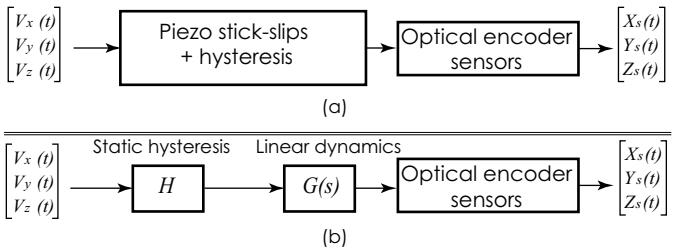

Figure 2: (a) Block diagram of the open-loop input/output transfers of X (resp. Y, Z) axis in scanning mode. (b) Using the Hammerstein model, a PSS actuator in scanning mode is equivalent to a static hysteresis followed by linear presliding dynamics.

3.1. Scanning mode dynamic modeling

The block diagram of Fig. 2(a) describes the open-loop system, where V_x (resp. V_y, V_z) is the input voltage and X_s(t) (resp. Y_s(t), Z_s(t)) is the slider displacement in X (resp. Y, Z) axis.

Each input/output transfer includes a hysteresis and a presliding dynamic between the PE and the slider. The hysteresis is the nonlinear relationship between the input voltage and the slider displacement. The Hammerstein model is used to describe the nonlinear dynamic in scanning mode as a static hysteresis H followed by a linear dynamic model $G(s)$ as shown in Fig. 2(b) [31]. This approximation is valid because the hysteresis does not affect the dynamic parameters such as the resonance frequencies and the damping.

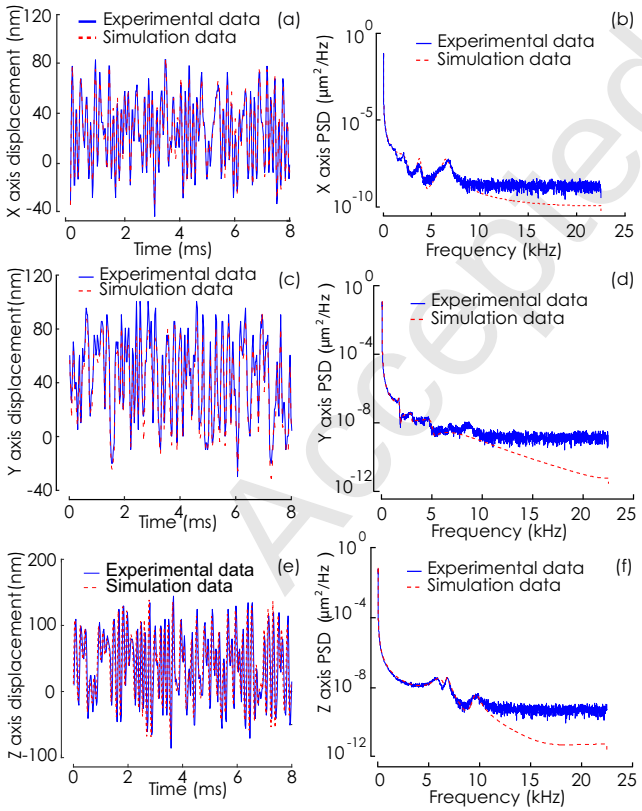

Figure 3: Experimental and identified linear presliding dynamics: (a) PRBS response of X axis, (b) Power Spectral Density (PSD) of X axis response , (c) PRBS response of Y axis, (d) PSD of Y axis response, (e) PRBS response of Z axis, (f) PSD of Z axis response [30].

3.1.1. Linear presliding dynamic modeling

The presliding dynamics are identified for each actuator using Pseudo-Random Binary Sequence (PRBS) signals, and modeled considering a linear parametric (an autoregressive-moving average with exogenous terms (ARMAX)) model. The model parameters are identified from the experimental data using the Matlab Identification ToolboxTM.

Fig. 3 shows experimental data and simulation data of the PRBS responses of X (resp. Y, Z) axis. Fig. 3(b) (resp. Fig. 3(d), Fig. 3(f))) shows that the PSS actuator in X (resp. Y, Z) axis has three resonance frequencies at 2061 Hz, 3652 Hz, and 6761 Hz (resp. 1684 Hz and 2870 Hz and 4397 Hz, 5819 Hz and 6760 Hz and 9613 Hz).

For an easy readability of the paper, in the sequel, the block diagrams will be presented for X axis only. Those of Y and Z axes can be obtained by replacing X by Y and Z, respectively.

3.1.2. MPI model of hysteresis

The modified Prandtl Ishlinskii (MPI) model is chosen because it is suitable for asymmetric hysteresis.

Unlike classical Prandtl Ishlinskii (PI) model which is composed of only backlash operators, the MPI model uses another type of operators, namely one-sided dead-zones, to catch the asymmetry [32]. This model is a superposition of weighted backlash operators followed by a superposition of dead-zone operators, where each backlash (resp. dead-zone) is characterized by a threshold $r_{X_{Si}}$ (resp. $r_{X_{Hi}}$) and a weighting coefficient $w_{X_{Hi}}$ (resp. $w_{X_{Si}}$) as shown in Fig .4.

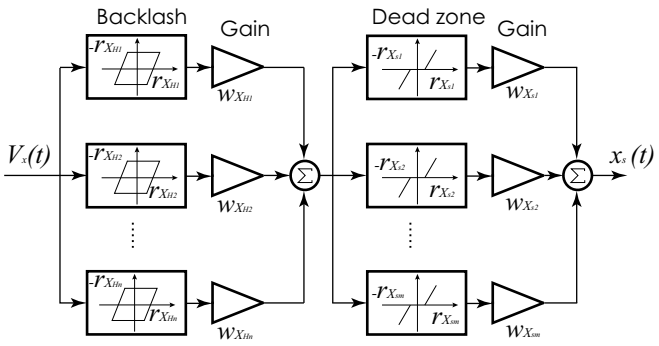

Figure 4: Block diagram of the MPI model.

To identify the MPI model parameters, sinusoidal voltage signals of different amplitudes and 50 Hz frequency are applied to the PSS actuators. The frequency is chosen so that the displacement is performed only in scanning mode. A number $n = 16$ of elementary backlashes and $m = 16$ of elementary dead-zone operators are defined. The thresholds have been initialized, and the weighting coefficients have been thereafter

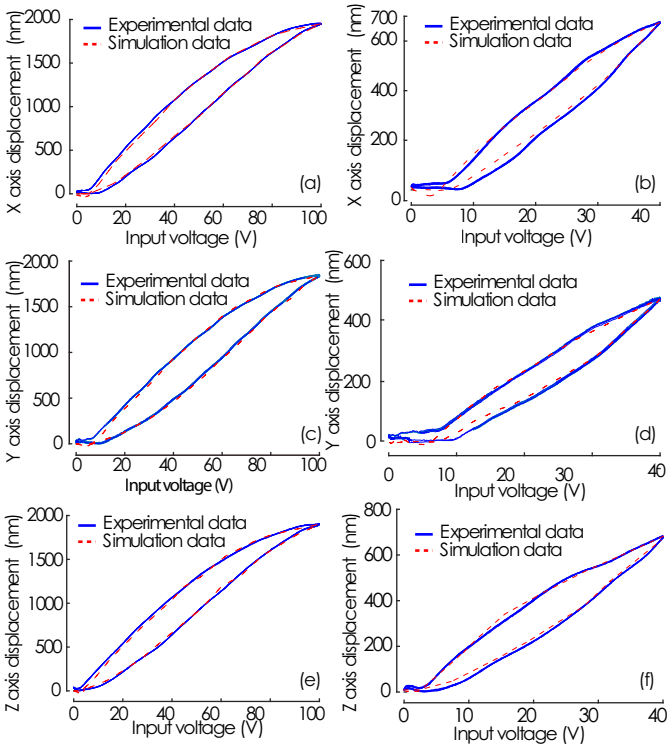

Figure 5: Experimental and identified MPI hysteresis. X axis for input signals of amplitudes: (a) 100 V, (b) 50 V. Y axis for input signals of amplitudes: (c) 100 V, (d) 50 V. Z axis for input signals of amplitudes: (e) 100 V, (f) 50 V [30].

identified using the Quadratic Programming Algorithm of the Matlab Optimization ToolboxTM.

Fig. 5 shows a good agreement between experimental and simulated hysteresis curves of the X, Y and Z axes, despite the small numbers of m and n.

3.1.3. Multi-linear approximation of hysteresis

The Multi-linear approximation of hysteresis is very suitable for the control design because it leads to a model with very few parameters [33]. In the $[V, X]$ plane, the hysteresis curve is

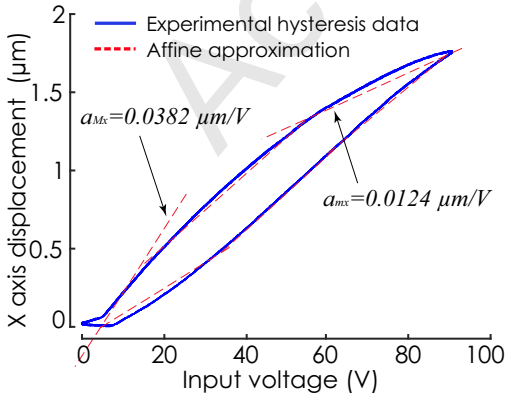

Figure 6: Multilinear approximation of hysteresis, and parameters estimation on X axis [30].

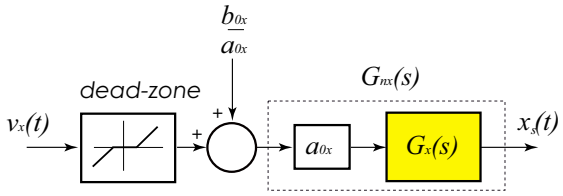

Figure 7: Block diagram of the PSS actuator with the multilinear approximation of hysteresis.

divided into several piecewise affine functions [34]. Fig. 6 illustrates this approximation using straight lines, where a_{Mx} and a_{mx} are the maximal and the minimal hysteresis slopes, respectively. Each hysteresis slope can be used for the control design.

The mean slope $a_{0x} = 0.0253\ \mu m//V$ is chosen to represent the static gain of the nominal model G_{nx} of the actuator as shown in Fig .7. As such, G_{nx} is the model whose frequency response is shown in Fig. 3 (b) but with a static gain equal to a_{0x}. In Fig .7, the ratio of b_{0x} on a_{0x} is an input disturbance [35]. The H_∞ control strategy, developed in the following section, is based on this model.

3.2. Scanning mode control

The scanning mode controller has to satisfy the following closed-loop specifications:

- ⊙ maximal closed loop response time lower than 5 ms,
- ⊙ vibrations damping with no overshoot,
- ⊙ maximal static error lower than 2%.

These control specifications are introduced through the following weighting functions:

- ⊙ W_{1x} to satisfy the tracking performances in terms of fast response time and low tracking error.
- ⊙ W_{2x} to keep the control voltage lower than 100 V.
- ⊙ W_{dx} to reduce the effect of the input disturbance $\frac{b_0}{a_0}$.
- ⊙ W_{tx} to reject the measurement noise $n(t)$.

3.2.1. H_∞ principle

The H_∞ optimization problem can be illustrated using the block diagram of Fig. 8, where $P(s)$ is the generalized plant model (i.e. the nominal model augmented by the weighting functions), $K(s)$ is the H_∞ controller, i are the exogenous inputs (e.g. reference signals, disturbances, noises,...etc), o are the exogenous outputs (e.g. errors or signals used in the optimization), ϵ are the available measurements, and u are the control signals.

$$F_l(P_x(s), K_x(s)) = \begin{pmatrix} W_{1x} \cdot S_x & -W_{1x} \cdot S_x \cdot G_{nx} \cdot W_{dx} & -W_{1x} \cdot S_x \\ W_{2x} \cdot K_x \cdot S_x & -W_{2x} \cdot T_x \cdot W_{dx} & -W_{2x} \cdot K_x \cdot S_x \\ W_{tx} \cdot T_x & W_{tx} \cdot S_x \cdot G_{nx} \cdot W_{dx} & -W_{tx} \cdot T_x \end{pmatrix} \quad (1)$$

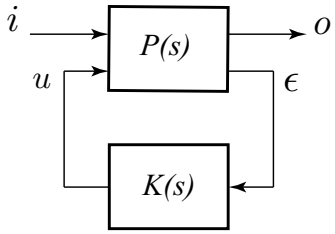

Figure 8: Block diagram of the general H_∞ problem.

The control objective is to find an optimal value γ and a controller $K(s)$, stabilizing internally the closed-loop system and guaranteeing the following inequality [36]:

$$\|F_l(P(s), K(s))\|_\infty < \gamma \quad (2)$$

Where $F_l(P(s), K(s))$ is defined as the transfer function between the exogenous outputs and the exogenous inputs. This transfer can be modified by the weighting functions used to introduce the desired closed-loop performance.

3.2.2. Robust H_∞ control

H_∞ problems are generally solved in form of the standard feedback control scheme illustrated in Fig. 9, where $x_s(t)$ denotes the PSS actuator position, and $x_r(t)$ the position reference.

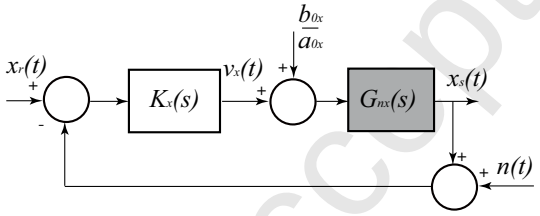

Figure 9: General feedback control scheme.

The closed-loop system augmented by the weighting functions is shown in Fig. 10. The transfer F_l between the exogenous inputs $(x_r\ d\ n)^T$ and the exogenous outputs $(e_1\ e_2\ e_3)^T$ is defined as shown in equations (1) and (3).

$S_x = (1+K_x \cdot G_{nx})^{-1}$ is the sensitivity function, and $T_x = (1+K_x \cdot G_{nx})^{-1} \cdot K_x \cdot G_{nx}$ is the complementary sensitivity function.

$$\begin{pmatrix} e_1 \\ e_2 \\ e_3 \end{pmatrix} = [F_l(P_x(s), K_x(s))] \begin{pmatrix} x_r \\ d \\ n \end{pmatrix} \quad (3)$$

As previously mentioned, the H_∞ problem consists in finding a controller $K_x(s)$ such that the inequality (4) is satisfied.

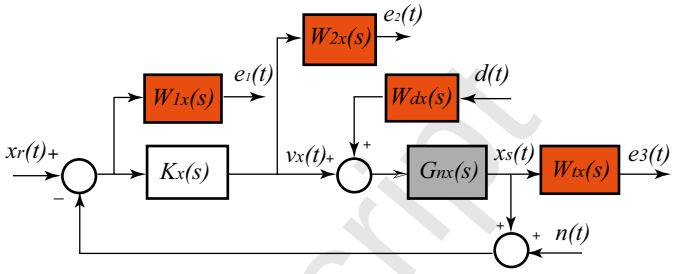

Figure 10: Closed-loop scheme with the weighting functions.

$$\|F_{l_{1-DOF}}(P_x(s), K_x(s))\|_\infty < \gamma_x \quad (4)$$

This amounts to meet the condition given in (5).

$$\begin{pmatrix} |S_x| < |\frac{\gamma_x}{W_{1x}}| & |S_x \cdot G_{nx}| < |\frac{\gamma_x}{W_{1x} \cdot W_{dx}}| & |S_x| < |\frac{\gamma_x}{W_{1x}}| \\ |K_x \cdot S_x| < |\frac{\gamma_x}{W_{2x}}| & |T_x| < |\frac{\gamma_x}{W_{2x} \cdot W_{dx}}| & |K_x \cdot S_x| < |\frac{\gamma_x}{W_{2x}}| \\ |T_x| < |\frac{\gamma_x}{W_{tx}}| & |S_x \cdot G_{nx}| < |\frac{\gamma_x}{W_{tx} \cdot W_{dx}} & |T_x| < |\frac{\gamma_x}{W_{tx}}| \end{pmatrix} \quad (5)$$

3.2.3. H_∞ control synthesis

The nonlinear static gain of PSS actuators comes from the hysteresis, and hence it takes values in the interval $[a_{mx}, a_{Mx}]$. Furthermore, the experimentation has shown a measurement delay. For the control design, this delay is considered varying in an interval $[0, T_r]$.

To take into consideration both the gain uncertainty and the time delay in the control design, PSS actuators are firstly modeled using the multilinear input uncertainty representation as shown in Fig. 11, where $W_{Ix}(s)$ is the uncertainty weighting function, and $\Delta_{Ix}(s)$ is the uncertainty defined as any stable transfer function with $|\Delta_{Ix}|(jw) \leq 1$ for all $w \in \mathbb{R}$.

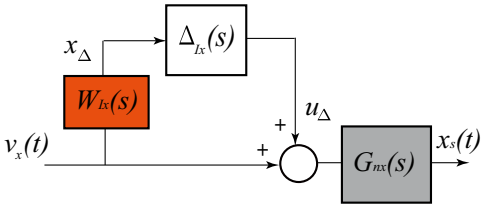

Figure 11: Block diagram of the PSS actuator with the multiplicative input uncertainty representation.

According to the small gain theorem, the closed-loop transfer x_Δ/u_Δ with the feedback H_∞ controller for any uncertain

plant $G_{px}(s) = G_{nx}(s)(1 + \Delta_{Ix}\omega_{Ix})$ can be written as in equation (6), where $T_{px} = (1 + K_x \cdot G_{px})^{-1} \cdot K_x \cdot G_{nx}$ is the complementary sensitivity function of the uncertain plant $G_{px}(s)$.

$$x_\Delta = -W_{Ix} \;\; T_{px}(s) \;\; u_\Delta \tag{6}$$

To satisfy robust stability against the gain uncertainties and the uncertain measurement delay, an additional constraint has to be taken into account in the H_∞ synthesis. This new constraint is obtained using the robust stability criterion as:

$$|T_{px}(s)| < \frac{1}{|w_{Ix}|} \qquad \forall w, \;\; \forall \, G_{px}(s) \tag{7}$$

Considering the weighting functions W_{1x}, W_{2x}, W_{dx}, W_{tx}, and W_{Ix} for each axis, and using the Riccati equation optimization algorithm [37], the H_∞ controllers have been designed for the three axes (X, Y, and Z) with a sampling frequency of 25 kHz. They are obtained with an optimal performance index of $\gamma_x = 1.9024$ for X axis, $\gamma_y = 2.1699$ for Y axis, and $\gamma_z = 2.1864$ for Z axis.

3.2.4. *Experimental results*

The H_∞ controllers are implemented on the 3-axes Cartesian system of Fig 1 with a sampling frequency of 25 kHz.

Experimental closed-loop step responses for input reference signals of 50 nm, 500 nm and 1 μm amplitudes are shown respectively in Fig. 12 (a), (c), and (e) for X axis, Fig. 13 (a), (c), and (e) for Y axis, and Fig. 14 (a), (c), and (e) for Z axis. The

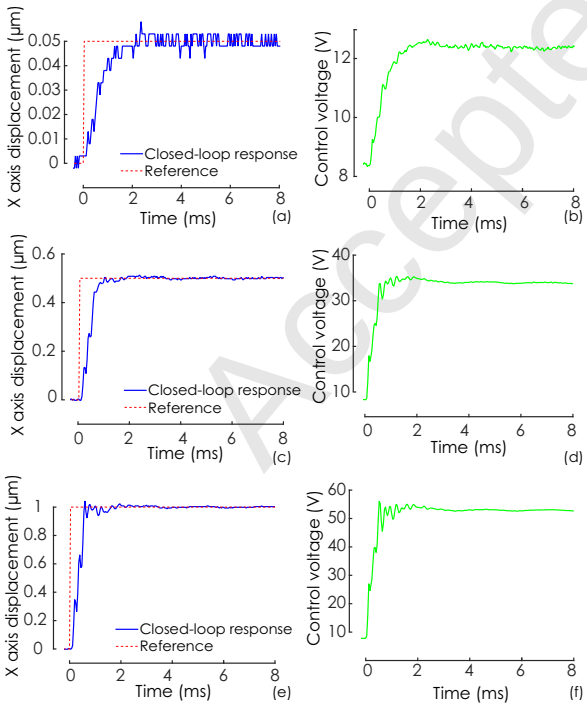

Figure 12: Experimental closed loop responses of X axis with the H_∞ controller. Reference signals of: (a) 1 μm, (c) 500 nm, and (e) 50 nm. Control voltages for reference signals of: (b) 1 μm, (d) 500 nm, and (f) 50 nm.

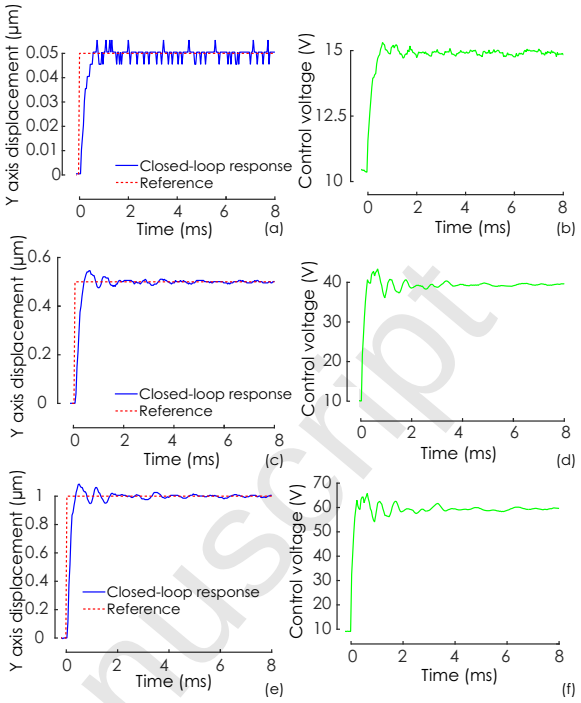

Figure 13: Experimental closed loop responses of Y axis with the H_∞ controller. Reference signals of: (a) 1 μm, (c) 500 nm, and (e) 50 nm. Control voltages for reference signals of: (b) 1 μm, (d) 500 nm, and (f) 50 nm.

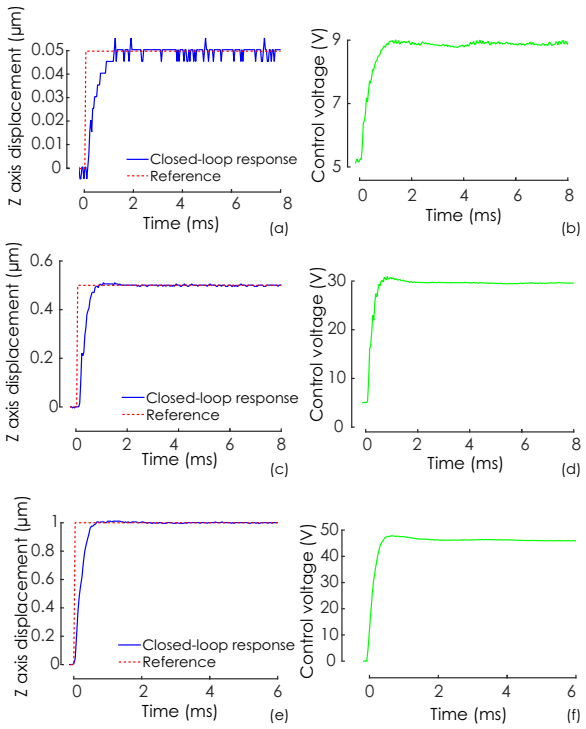

Figure 14: Experimental closed loop responses of Z axis with the H_∞ controller. Reference signals of: (a) 1 μm, (c) 500 nm, and (e) 50 nm. Control voltages for reference signals of: (b) 1 μm, (d) 500 nm, and (f) 50 nm.

corresponding control voltages are illustrated in Fig. 12 (b), (d), and (f) for X axis, Fig. 13 (b), (d), and (f) for Y axis, and Fig. 14 (b), (d), and (f) for Z axis.

The closed loop response times for reference signals of 1 μm and 500 nm amplitudes are respectively 1.2 ms, 0.8 ms for X axis, 1.2 ms, 1.1 ms for Y axis, and 0.5 ms, 0.4 ms for Z axis. In the dynamic mode, the overshoots are significantly reduced, and for reference signals of 1 μm and 500 nm amplitudes, they are respectively equal to 4.3 %, 0.5 % for X axis, 8.6 %, 8.2 for Y axis, and 0.6 %, 0.4 % for Z axis. The static error is close to zero and it is less than 1.2 % for the three axis and 1 μm and 500 nm amplitudes reference signals.

Response times, overshoots, and static errors are not given for the 50 nm amplitude reference signals as the sensor noise is significant in the corresponding step responses.

Closed-loop tracking of a circle with X and Y axes is performed experimentally. Different sine reference signals of 1μm amplitude and fixed frequencies, namely 1 Hz, 10 Hz, 50 Hz, 100 Hz, 200 Hz, 300 Hz, 350 Hz, and 400 Hz, are used. Experimental results are shown in Fig. 15.

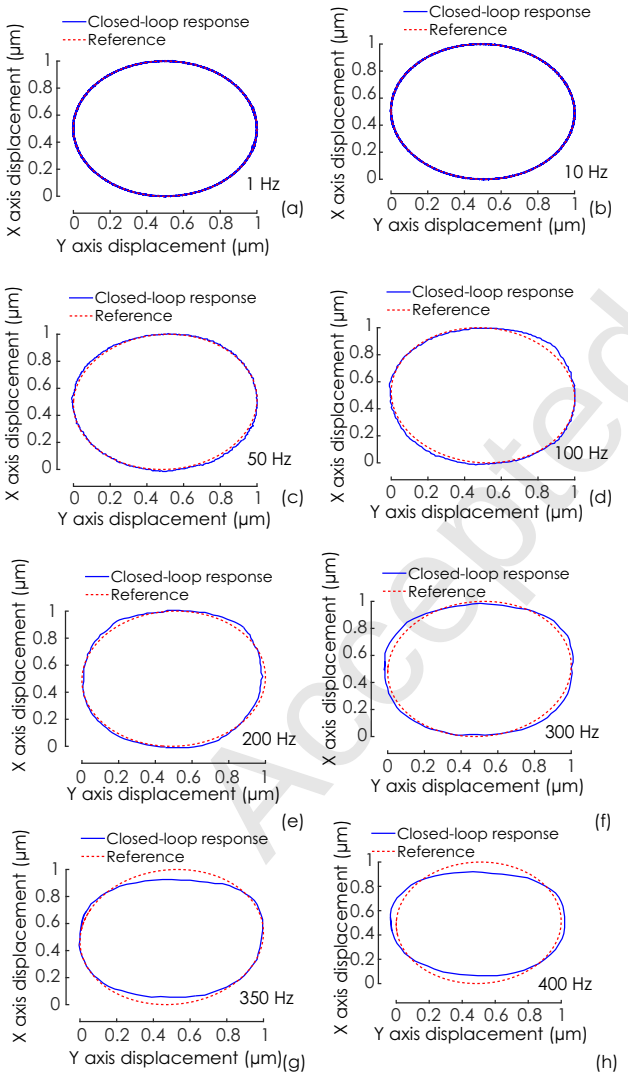

Figure 15: Experimental tracking of a circle by XY axes with the H_∞ controller: (a) 1 Hz, (b) 10 Hz, (c) 50 Hz, (d) 100 Hz, (e) 200 Hz, and (f) 300 Hz, (g) 350 Hz, and (h) 400 Hz.

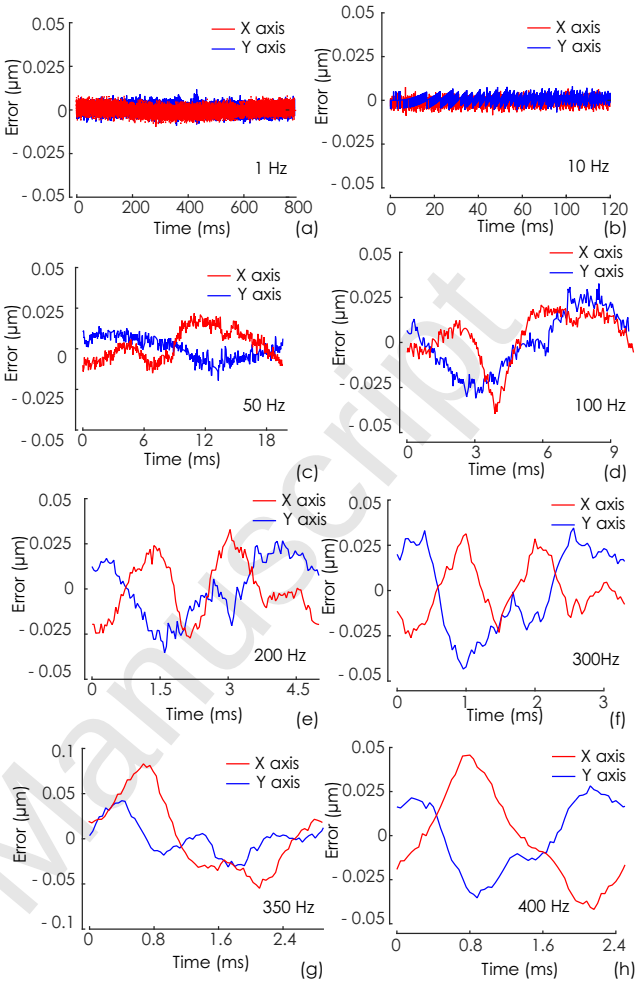

Figure 16: Experimental errors in XY axes in closed-loop with the H_∞ controller when tracking a circle with frequencies: (a) 1 Hz, (b) 10 Hz, (c) 50 Hz, (d) 100 Hz, (e) 200 Hz, (f) 300 Hz, (g) 350 Hz, and (h) 400 Hz.

The experimental tracking error is illustrated in Fig. 16 for X and Y axes and for the different tracking frequencies. The maximum error respectively for X and Y axes are 0.7 % and 1.18 % for 1 Hz, 0.9 % and 0.74 % for 10 Hz, 2 % and 1.9 % for 50 Hz, 4.29 % and 3.2 % for 100 Hz, 3.33 % and 2.6 % for 200 Hz, 3.1 % and 4.3 % for 300 Hz, 7.9 % and 4.2 % for 350 Hz, 9.5 % and 7.1 % for 400 Hz. This error is less than 5 % for trajectory tracking up to 300 Hz with both X and Y axes. Y axis is able to track trajectories up to 350 Hz with less than 5 % tracking error as it has a faster rising time than that of X axis. The rising time is 0.3 ms for Y axis whereas it is 0.6 ms for X axis.

These results demonstrate the ability of the closed-loop system to track trajectories at frequencies up to 300 Hz with a tracking error less than 5 % .

Fig. 17 illustrates the closed-loop response of X axis for a

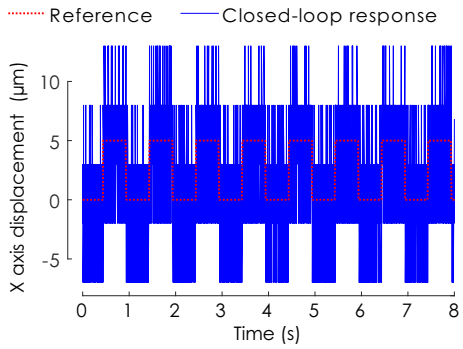

Figure 17: X axis closed-loop response for a reference square signal of 5 nm amplitude with the scanning controller.

square reference signal of 5 nm amplitude. This experimental displacement curve shows the achievable positioning resolution of these actuators in scanning mode using the H_∞ controllers.

4. Control in stepping mode

The objective of the stepping mode control is to perform a positioning with a large range displacement, i.e micrometer and millimeter ranges. To this end, a f/u proportional control strategy [29] is designed.

4.1. Mixed stepping / scanning dynamic modeling

The open-loop system is illustrated in Fig. 18, where $x_p(t)$ and $x_s(t)$ are respectively the PE and the slider displacements, $v_x(t)$ is the input voltage of the PE and $F_f(t)$ is the friction force between the PE and the slider. C_H is a static conversion coefficient. The nonlinear model involves the static hysteresis H, the dynamic model of the PE and that of the slider and the nonlinear dynamic of the friction force. More details about the non-linear mixed stepping/scanning modeling can be found in the previous work [38]. This model is well adapted for the definition of stepping control parameters.

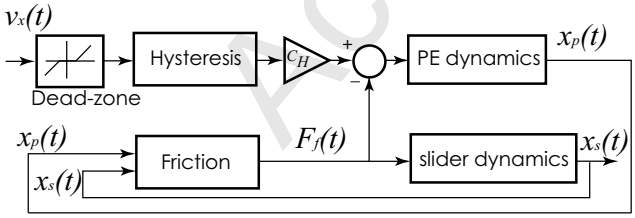

Figure 18: Block diagram of the open-loop input/output transfer in stepping mode.

4.2. Stepping mode control

4.2.1. f/u proportional control

The closed-loop f/u proportional control scheme is shown in Fig. 19. It includes the PSS actuator to be controlled, a home made sawtooth generator based on an *arduino due*, an amplitude proportional controller gain K_{ux} and a frequency proportional controller gain K_{fx}.

The sawtooth generator has three inputs, namely the voltages $u_x(t)$, $f_x(t)$ and $d_x(t)$ to set respectively the amplitude, the frequency and the direction of the sawtooth voltage $v_x(t)$ at each sampling time. The amplitude and the frequency of $v_x(t)$ can vary in the ranges [0 - 5V] and [few Hz - 20 kHz] respectively. The voltage $v_x(t)$ is amplified by a linear amplifier with a gain of 20 to feed the PE.

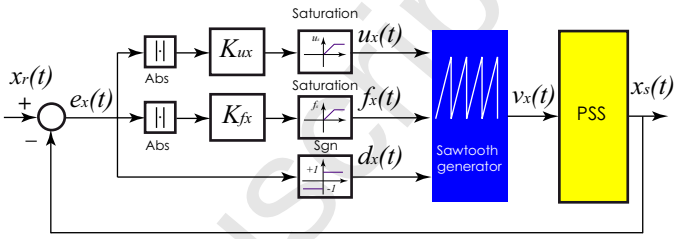

Figure 19: Closed-loop f/u proportional control scheme of the PSS actuator in stepping mode.

4.2.2. Experimental results

The f/u proportional controllers are designed for the three axes of the Cartesian nano-robot (Fig. 1). The control gains K_{ux} and K_{fx} are defined experimentally by trial and error to have a good compromise between the positioning precision and the vibration damping. The gains have been defined for a position reference of 1 *mm* and the same gains have been used for all the experiments performed thereafter, i.e. for different input references and for the three nano-robot axes. The sampling frequency is 25 kHz.

Step references of 1 *mm*, 100 μm, 50 μm, and 5 μm are used for the validation. Fig. 20 shows experimental results for X axis. The response time is equal to 26.9 ms (resp. 3.8 ms, 2.5 ms, 2.4 ms) for a reference signal of 1 *mm* (resp. 100 μm, 50 μm, and 5 μm) amplitude. Fig. 21 shows the experimental results for Y axis. The response time is equal to 40.7 ms (resp. 4.7 ms, 2.8 ms, 2.7 ms) for a reference signal of 1 *mm* (resp. 100 μm, 50 μm, and 5 μm) amplitude. Fig. 22 shows the experimental results for Z axis. The response time is equal to 27.7 ms (resp. 3.4 ms, 1.9 ms, 1.1 ms) for a reference signal of 1 *mm* (resp. 100 μm, 50 μm, and 5 μm) amplitude. Static errors are close to zero for the three axes and for the reference signals of different amplitudes. The displacement curves are smooth thanks to the ability of the *arduino due* card and the defined algorithm to generate sawtooth voltages at relatively high frequencies up to 20 kHz. As such, the stick and slip phases are almost invisible.

The f/u proportional controller always feed the actuator with a sawtooth voltage. It ensures good tracking performances but for displacements lower than the maximum elongation of the PE, i.e. less than 2 μm. In this case, the scanning controller provides better positioning results mainly in terms of resolution as it will be shown in the sequel. In an ideal case, a global

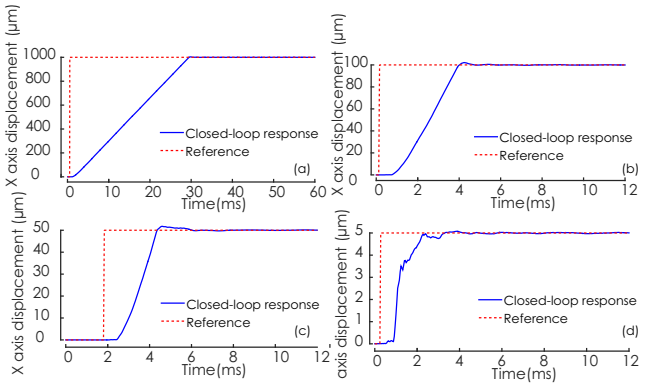

Figure 20: Experimental displacement of the X axis in closed-loop with the f/u proportional controller for step reference signals of amplitude: (a) 1000 μm, (b) 100 μm, (d) 50 μm, and (e) 5 μm.

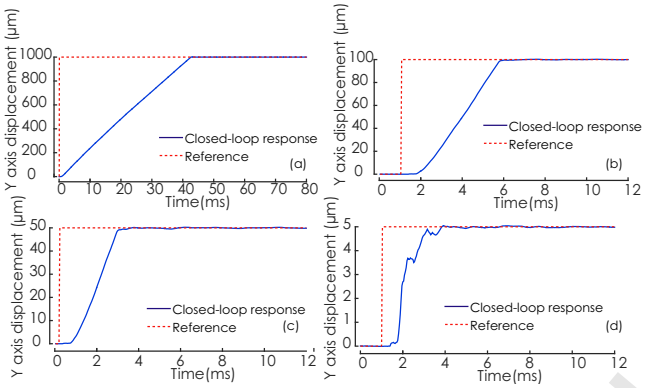

Figure 21: Experimental displacement of the Y axis in closed-loop with the f/u proportional controller for step reference signals of amplitude: (a) 1000 μm, (b) 100 μm, (d) 50 μm, and (e) 5 μm.

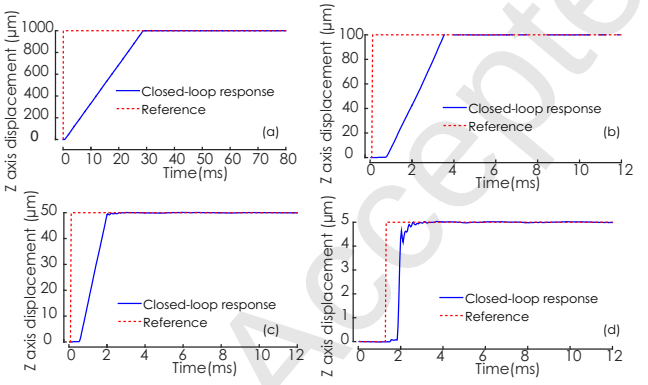

Figure 22: Experimental displacement of the Z axis in closed-loop with the f/u proportional controller for step reference signals of amplitude: (a) 1000 μm, (b) 100 μm, (d) 50 μm, and (e) 5 μm.

control structure should be able to switch between the stepping controller to the scanning controller when the required displacements are in the range of the elongation of the PE. This switch must be transparent for the user. In other words, the aim is to be able to perform positioning tasks with millimeter or micrometer range displacements and a nanometer resolution without worrying about the mode of operation of the actuator.

5. Mixed stepping/scanning mode control

5.1. Switching control problem

To deal with the transition between the coarse and the fine positioning of the nano-robot in a transparent way, a switch control strategy between the stepping and the scanning controllers in needed. Even if the switch is stable, the bump transfer at switching time can generate undesired vibrations of the actuator due to the discontinuity of the control voltage of the two controllers. The generated oscillations can damage the end effector of the nano-robot or the object to be manipulated.

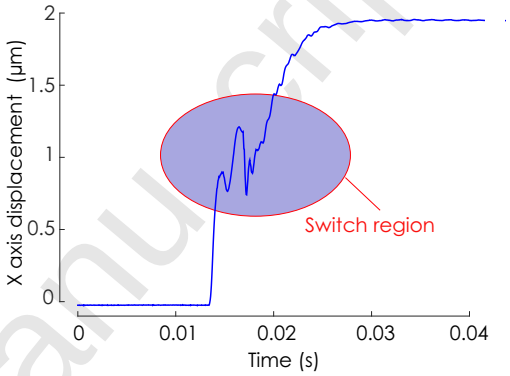

Figure 23: The closed-loop X axis displacement with the controller provided by SmarAct company. The maximum elongation of the PE is between 1 μm and 1.5 μm while the input reference is 2 μm. When the position of the slider exceeds the maximum elongation of the PE, vibrations are produced due to a slip phase.

For instance, Let us consider the mechanical characterization task of mico-membranes of [12]. The end effector is a tungsten probe attached on the Z axis. It is brought close to the micro-membrane in a semi-automated way: (i) It is approached from few millimeters distance to few micrometers distance in a coarse mode. (ii) It is thereafter controlled using the SmarAct controller to bring it from few micrometer distance to few nanometers distance. This characterization gives satisfactory results, but it is time consuming. Moreover the transition from stepping mode to scanning mode generate significant vibrations of around 100 nm as shown in Fig. 23 while the micro-membranes are 200 nm thin.

5.2. Control principle

Switched controllers have to provide control outputs with an equal first derivative at the switching time to avoid a bump transfer. The issue for PSS actuators is that it is necessary to deal with a system that has two operating modes. The first one is the scanning mode alone. The second is the stepping mode that includes a succession of scanning modes.

The structure of the proposed mixed stepping/scanning mode control is shown in Fig. 24. It includes the H_∞ scanning controller, the f/u proportional stepping controller and the internal

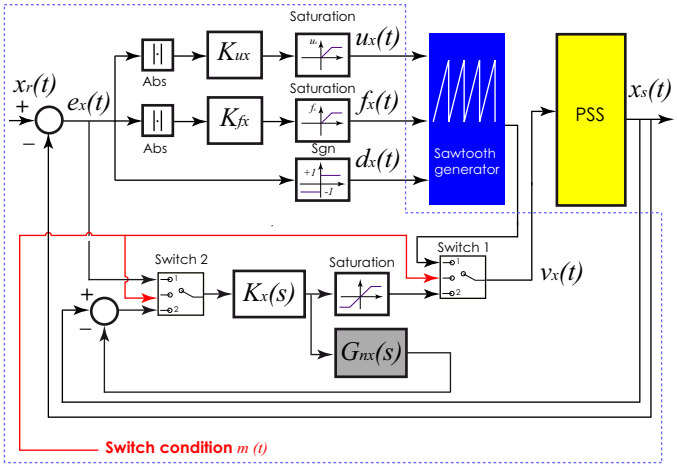

Figure 24: The mixed stepping/scanning control strategy for PSS actuators. The dashed bloc includes the elements that are implemented in the processor board for the experimental validation.

model of the actuator $G_{nx}(s)$ to deal with the bumpless switching. The aim is to to mitigate vibrations at the switching time and to satisfy closed-loop stability.

Each PSS actuator can be controlled as follows:

***-Stepping mode control-*:** the PSS actuator is initially controlled using the f/u proportional controller designed in section 4. The nominal model $G_{nx}(s)$ (see section 3.1.3) is meanwhile used when the scanning controller K_x is offline. In this case, the position reference of the offline controller is the current position $x_s(t)$ of the actuator. During the Stepping control, the Switch 1 is on position 1 and and the Switch 2 is on position 2. The switch condition is defined by the user.

***- Mixed stepping/scanning mode control-*:** Thanks to the closed-loop system composed of K_x and G_{nx} with the reference position x_s, during the stepping mode control, the control voltage value of the scanning mode controller approaches that of the stepping mode controller so that at switching time, the transition between the two control voltages is smooth.

***-Scanning mode control-*:** the Switch 1 is on position 2 and Switch 2 is on position 1. The actuator is controlled in scanning mode only using the H_∞ controller designed in section 3.2.2. The position reference is in this case x_r. Precise and fast positioning of the actuator can be achieved.

The mixed structure presented above can simultaneously manage the two operating modes of the actuator. Its main advantage consists in the fact that the user has not to specify the well-suited operating mode according to the desired task, as it is automatically done by the mixed control strategy. This is a novelty in control of PSS actuators. Experimental validations are presented in the following section.

5.3. Experimental results

The real time implementation of the control is done on X and Y axes of the Cartesian nano-robotic system of Fig. 1. The

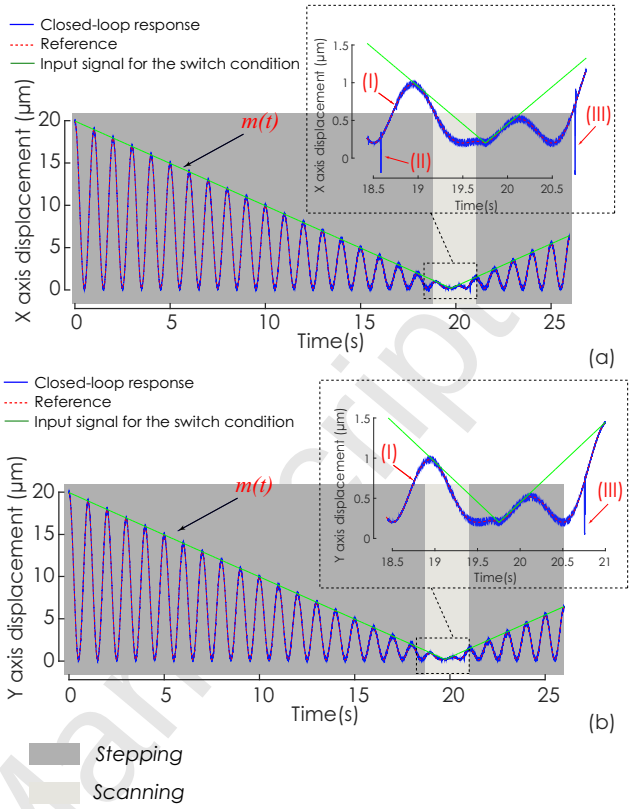

Figure 25: Closed loop response of X axis (a) and Y axis (b) to a 1 Hz sinusoidal reference position with a deceasing amplitude. The switch from the stepping mode to the scanning mode happens when the input signal $m(t)$ for the switch condition is less than 1.2 μm.

latter is operating inside the SEM vacuum chamber.

The parts inside the dashed bloc of Fig. 24 are implemented on the processor board. Different parameters such as those of the reference signal $x_r(t)$ and the switch condition can be set and changed in real time thanks to the human-machine interface. The signals $u_x(t)$, $f_x(t)$ and $d_x(t)$ are calculated by the controller and connected at the input of the sawtooth generator through DAC (Digital To Analog) converters of 16 bit resolution and 1.6 μs sample time. The current position of the actuator measured by the integrated optical encoder is fed back to the controller thanks to a an incremental encoder interface board.

The reference trajectory selected for the experimental test of the mixed controller is a sinusoidal signal of 1 Hz frequency and a decreasing amplitude from 20 μm to less than 1 μm as shown in Fig. 25. Let $m(t)$ be the straight line passing through the peaks of the reference signal (Fig. 25). The switch from the stepping control to the scanning control is performed when $m(t) < 1.2\ \mu m$. The controller is implemented with 25 kHz sampling frequency.

Experimental results are presented in Fig. 25 (a) Fig. 25 (b) and for X and Y axes respectively. The nano-robot axes are actuated with the f/u proportional controller when $m(t) >= 1.2\ \mu m$ and with the H_∞ controller otherwise. Three main vibrations

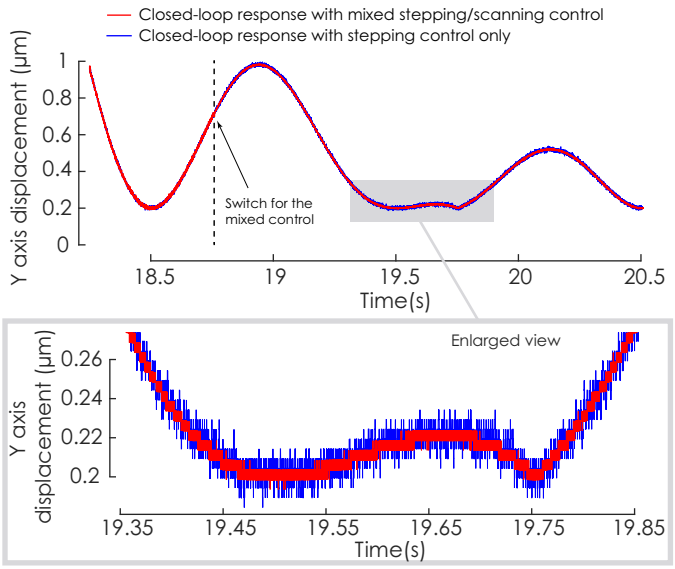

Figure 26: Closed-loop response of Y axis with the mixed stepping/scanning control and the stepping control only.

can be observed as shown in Fig. 25. The vibration (I) is due to the switch from the stepping to the scanning controller. Its amplitude is lower than 80 *nm* for X axis and almost unobservable for Y axis. The vibration (II) happens during the stepping control, it is due to the slip phase when the PE exceeds its maximum elongation. The vibration (III) is due to the switch from the scanning to the stepping controller. This vibration occurs since the bumpless switch from the scanning to the stepping mode control is not considered in this paper.

Some experimental issues occur. The results of Fig. 25 are not always reproducible. For instance, if the switch from the stepping to the scanning mode control happens when the control voltage is close to 0 V or 100 V (i.e. the limits of input voltage of the PE), the PE has not enough displacement range to follow the reference trajectory. In this case the switch is produced with vibrations. This is one of the probable reasons of the reproducibility issue. Nevertheless, several experiments have given very satisfactory results similar to those of Fig. 25. The reproducibility of the experiments will be investigated in future works.

In a second time, the nano-robot axes are controlled only in stepping mode (i.e. without switch) for the same reference position $x_r(t)$. The results for Y axis are presented in Fig. 26 and compared with those obtained using the mixed stepping / scanning control. For displacements lower than 1 μm, the use of a scanning control (H_∞ in the case of the study) allows reaching the sensor resolution (i.e. 5 nm), while the resolution obtained if only the stepping control is used is around 25 nm. The other advantage to use a scanning controller in the fine positioning mode and hence a switch strategy is that it offers the possibility to set precisely the closed loop specifications during the control design which is not the case when the actuator is controlled with only a sawtooth type voltage.

Experimentations have shown that the new mixed stepping/scanning control strategy can perform stable and smooth switch between two controllers of different structures. This controller can guarantee fully-automated nano-robotic applications when millimeter or micrometer range displacements with a nanometer resolution are required.

6. Conclusion

Nanotechnologies are increasingly requiring robotics at the nanometer scale. SEM-integrated nano-robotic systems have therefore emerged to perform the main required tasks, such as nano-manipulation, nano-assembly, electrical characterization and mechanical characterizations. The PSS actuator is one of the best candidates in nano-robotics because it is able to perform long-range coarse displacements in stepping mode and fine displacements with a nanometer resolution in scanning mode. Control of these actuators is challenging due to several reasons among which the hybrid stepping/scanning operating modes. This paper has focused on the control of PSS actuators to perform large range motions with a nanometer range resolution. A H_∞ controller has been firstly designed in scanning mode to satisfy multi-objective criteria in terms of stability robustness w.r.t hysteresis and the measurement time delay, closed loop bandwidth and precision. A f/u proportional controller has then been designed to control the actuators in a large motion range in stepping mode. A new mixed control strategy able to switch from the stepping control mode to the scanning control mode has been thereafter proposed to drive the PSS actuators in a mixed stepping/scanning operating mode. Experimental results have demonstrated the effectiveness of the controller and have therefore opened new perspectives for the capability of automated nano-robotics. Futur works will concern the extension of the control method to deal with tracking performance of the switch from the scanning mode to the stepping mode.

7. Acknowledgment

The authors would like to thank Georges Daher, phd student at Sorbonne Université, for the complete design and programming of the sawtooth generator based on *arduino due*. This work has been partially sponsored by the French government research program Investissements d'avenir through the Robotex Equipment of Excellence (ANR-10-EQPX-44)

References

[1] M. Takahashi, H. Ko, T. Ushiki, F. Iwata, Interactive nano manipulator based on an atomic force microscope for scanning electron microscopy, International Symposium on Micro-NanoMechatronics and Human Science (MHS) (2011) 495–500.

[2] S. Qin, T. Kim, Z. Wang, A. Li, Nanomanipulation and nanofabrication with multi-probe scanning tunneling microscope: From individual atoms to nanowires, Review of Scientific Instruments 83 (6) (2012) 063704.

[3] V. Eichhorn, M. Bartenwerfer, S. Fatikow, Nanorobotic assembly and focused ion beam processing of nanotube-enhanced afm probes, IEEE Transactions on Automation Science and Engineering 9 (4) (2012) 679–686.

[4] Z. Yang, M. Nakajima, Y. Shen, T. Fukuda, Assembly and evaluation of mwcnts probe thermal sensor by nanorobotic manipulation, 12th IEEE Conference on Nanotechnology (2012) 1–4.

[5] Y. Zhang, Z. Liang, R. Yong, C. Changhai, K. Brandon, Y. Sun, A load-lock-compatible nanomanipulation system for scanning electron microscope, IEEE/ASME Transactions on Mechatronics 18 (1) (2013) 230–237.

[6] S. Boles, A. Sedlmayr, O. Kraft, R. Mönig, In situ cycling and mechanical testing of silicon nanowire anodes for lithium-ion battery applications, Applied Physics Letters 100 (24) (2012) 243901.

[7] C.Ru, Y. Zhang, Y. Sun, Y. Zhong, X. Sun, D. Hoyle, I. Cotton, Automated four-point probe measurement of nanowires inside a scanning electron microscope, IEEE Transactions on Nanotechnology 10 (4) (2011) 674–681.

[8] Y. Wang, J. Zhu, M. Pang, J. Luo, S. Xie, M. Liu, L. Sun, C. Zhou, , M. Tan, J. Ge, et al., A stick-slip positioning stage robust to load variations, IEEE/ASME Transactions on Mechatronics 21 (4) (2016) 2165–2173.

[9] G.-Y. Gu, L.-M. Zhu, C.-Y. Su, H. Ding, S. Fatikow, Modeling and control of piezo-actuated nanopositioning stages: A survey, IEEE Transactions on Automation Science and Engineering 13 (1) (2016) 313–332.

[10] Y. Li, Q. Xu, Adaptive sliding mode control with perturbation estimation and pid sliding surface for motion tracking of a piezo-driven micromanipulator, IEEE Transactions on Control Systems Technology 18 (4) (2010) 798–810.

[11] T. Lu, M. Boudaoud, D. Hériban, S. Régnier, Nonlinear modeling for a class of nano-robotic systems using piezoelectric stick-slip actuators, IEEE/RSJ International Conference on Intelligent Robots and Systems (2015) 6020–6025.

[12] J. Abrahamians, B. Sauvet, J. Polesel-Maris, R. Braive, S. Régnier, A nanorobotic system for in situ stiffness measurements on membranes, IEEE Transactions on Robotics 30 (1) (2014) 119–124.

[13] G. Wang, G. Chen, F. Bai, High-speed and precision control of a piezoelectric positioner with hysteresis, resonance and disturbance compensation, Microsystem Technologies 22 (10) (2016) 2499–2509.

[14] G.-Y. Gu, L.-M. Zhu, C.-Y. Su, Modeling and compensation of asymmetric hysteresis nonlinearity for piezoceramic actuators with a modified prandtl–ishlinskii model, IEEE Transactions on Industrial Electronics 61 (3) (2014) 1583–1595.

[15] X. Zhou, J. Zhao, G. Song, J. A. De Abreu-Garcia, Preisach modeling of hysteresis and tracking control of a thunder actuator system, Smart Structures and Materials 2003: Modeling, Signal Processing, and Control 5049 (2003) 112–126.

[16] K. Kuhnen, H. Janocha, Inverse feedforward controller for complex hysteretic nonlinearities in smart-material systems, Control and Intelligent Systems 29 (3) (2001) 74–83.

[17] M. Rakotondrabe, Bouc–wen modeling and inverse multiplicative structure to compensate hysteresis nonlinearity in piezoelectric actuators, IEEE Transactions on Automation Science and Engineering 8 (2) (2011) 428–431.

[18] S. R. Moheimani, A survey of recent innovations in vibration damping and control using shunted piezoelectric transducers, IEEE transactions on control systems technology 11 (4) (2003) 482–494.

[19] M. Rakotondrabe, C. Clévy, P. Lutz, Complete open loop control of hysteretic, creeped, and oscillating piezoelectric cantilevers, IEEE Transactions on Automation Science and Engineering 7 (3) (2010) 440–450.

[20] L. Li, C.-X. Li, G. Gu, L.-M. Zhu, Positive acceleration, velocity and position feedback based damping control approach for piezo-actuated nanopositioning stages, Mechatronics 47 (2017) 97 – 104.

[21] A. J. Fleming, S. S. Aphale, S. R. Moheimani, A new method for robust damping and tracking control of scanning probe microscope positioning stages, IEEE Transactions on Nanotechnology 9 (4) (2010) 438–448.

[22] M.-S. Tsai, J.-S. Chen, Robust tracking control of a piezoactuator using a new approximate hysteresis model, Journal of dynamic systems, measurement, and control 125 (1) (2003) 96–102.

[23] A. Sebastian, S. M. Salapaka, Design methodologies for robust nanopositioning, IEEE Transactions on Control Systems Technology 13 (6) (2005) 868–876.

[24] M. Al Janaideh, M. Rakotondrabe, O. Aljanaideh, Further results on hysteresis compensation of smart micropositioning systems with the inverse prandtl–ishlinskii compensator, IEEE Transactions on Control Systems Technology 24 (2) (2016) 428–439.

[25] H. C. Liaw, B. Shirinzadeh, J. Smith, Enhanced sliding mode motion tracking control of piezoelectric actuators, Sensors and Actuators A: Physical 138 (1) (2007) 194–202.

[26] I. R. Petersen, H. R. Pota, Minimax LQG optimal control of a flexible beam, Control Engineering Practice 11 (11) (2003) 1273–1287.

[27] J.-M. Breguet, R. Clavel, Stick and slip actuators: design, control, performances and applications, Micromechatronics and Human Science, 1998. MHS'98. Proceedings of the 1998 International Symposium o.

[28] B. Sedghi, Control design of hybrid systems via dehybridization, EPFL.

[29] M. Rakotondrabe, Y. Haddab, P. Lutz, Voltage/frequency proportional control of stick-slip micropositioning systems, IEEE Transactions on Control Systems Technology 16 (6) (2008) 1316–1322.

[30] R. Oubellil, A. Voda, M. Boudaoud, S. Régnier, A 2-dof H_∞ control strategy for a 3 axes robotic system operating at the nanometer scale, 20th International Conference on System Theory, Control and Computing (ICSTCC) (2016) 355–362.

[31] S. Billings, Identification of nonlinear systems–a survey, IEE Proceedings D (Control Theory and Applications) 127 (6) (1980) 272–285.

[32] K. Kuhnen, Modeling, identification and compensation of complex hysteretic nonlinearities: A modified prandtl-ishlinskii approach, European journal of control 9 (4) (2003) 407–418.

[33] M. Grossard, M. Boukallel, N. Chaillet, C. Rotinat-Libersa, Modeling and robust control strategy for a control-optimized piezoelectric microgripper, IEEE/ASME Transactions On Mechatronics 16 (4) (2011) 674–683.

[34] M. Rakotondrabe, Y. Haddab, P. Lutz, Quadrilateral modelling and robust control of a nonlinear piezoelectric cantilever, IEEE Transactions on Control Systems Technology 17 (3) (2009) 528–539.

[35] R. Oubellil, A. Voda, M. Boudaoud, S. Régnier, Robust control strategies of stick-slip type actuators for fast and accurate nanopositioning operations in scanning mode, 23th Mediterranean Conference on Control and Automation (MED) (2015) 650–655.

[36] P. Apkarian, Elements de la théorie de la commande robuste.

[37] J. C. Doyle, K. Glover, P. P. Khargonekar, B. A. Francis, State-space solutions to standard H_2 and H_∞ infinity/control problems, IEEE Transactions on Automatic control 34 (8) (1989) 831–847.

[38] M. Boudaoud, S. Liang, T. Lu, R. Oubellil, S. Régnier, Voltage/frequency rate dependent modeling for nano-robotic systems based on piezoelectric stick-slip actuators, IEEE/RSJ International Conference on Intelligent Robots and Systems (IROS) (2016) 5297–5303.

Highlights

- Comprehensive modeling of Piezoelectric Stick-Slip (PSS) actuators to accurately describe both scanning and stepping operating modes.
- A multi-criteria robust control strategy in scanning mode ensures positioning with motion range from few nanometers to few micrometers, and nanometer resolution.
  - It satisfies a good compromise between closed-loop bandwidth and vibration damping.
  - It guarantees stability robustness against hysteresis and uncertain measurement time-delay.
- A frequency/amplitude controller ensures precise positioning with displacement range from few tens micrometers to few millimeters.
- A new mixed stepping/scanning mode control strategy guarantees accurate positioning with displacement range from few nanometers to few millimeters.
  - It is able to switch between the scanning and stepping modes while guaranteeing closed-loop stability and bumpless at switching time.
  - It opens new perspectives to the use of the PSS actuators in fully-automated nano-robotic applications inside a Scanning Electron microscope (SEM).

Authors biography

Raouia Oubellil received an engineer degree in control systems from National polytechnic school of Algiers, Algeria, in 2012. She is also graduated master 2 Research in control systems, signal and image processing from Ecole Normale Superieure de Cachan, Paris, France, in 2013. She obtained a PhD degree in control systems from the University of Grenoble Alpes, in 2016. She is actually a teaching assistant at the University of Franche-Comté (UFC), and a research assistant at FEMTO-ST Institute, Besanon, France. Her primary research interest is in robust control. More specifically, robust control of a nanorobotics system.

Alina Voda received the Diploma degree in energy engineering from the Polytechnical University of Bucarest, Bucarest, Romania, and the Ph.D. degree in control from the Polytechnical Institute of Grenoble, Grenoble, France, in 1987 and 1994, respectively. She was a Nuclear Power Engineer with Cernavoda Nuclear Plant, and then with the Research Center for Energy, Bucarest, until 1990. She was an Assistant Professor in control with University Joseph Fourier, Grenoble, in 1995, where she is still serving as an Associate Professor. She was also with Pechiney Research Center, Voiron, France, in 2001. Her current research interests are held at the Control Systems Department of GIPSA-lab and cover various control/identification problems, as well as different application fields either in

industry or in sciences (electro-mechanical systems, micro/nano-sciences).

Mokrane Boudaoud received the engineering degree in automatic control from the University of science and technology Houari Boumédiène (USTHB, Algiers, Algeria), and a MS degree in mechatronics and microrobotics at the University of Franche-Comté (UFC, Besanon, France) in 2009. He received in 2012 the PhD degree in control engineering at AS2M (Automatic Control and Micro-Mechatronic Systems) department of Femto-st Institute. He is currently Associate Professor at University Pierre et Marie Curie / Institut des Systèmes Intelligents et de Robotique. His field of interest includes modeling and robust control of multi-degree-of-freedom nano-robotic systems operating under a scanning electron microscope (SEM).

Stéphane Régnier received his PhD degree in Mechanics and Robotics from the University of Pierre and Marie Curie, Paris, France in 1996. He is currently Professor at the Institute of Intelligent Systems and Robotics (ISIR), University of Pierre and Marie Curie, Paris, France. He has been head of the ISIR micromanipulation team since 2001. His research interests are focused on micro and nano manipulation, teleoperation and haptic feedback at the nanoscale, micromechatronics and biological cell characterization.